Modeling of radiation heat transfer in dense-bed flows of solids in indirectly heated rotary kilns

S. Tavakkol* [1], T. Zirwes [2,3], J.A. Denev [2], H. Bockhorn [3], D. Stapf [1]
*Salar.Tavakkol@kit.edu
1 Karlsruhe Institute of Technology, Institute of Technical Chemistry, Eggenstein-Leopoldshafen
2 Karlsruhe Institute of Technology, Steinbuch Centre for Computing, Eggenstein-Leopoldshafen
3 Karlsruhe Institute of Technology, Engler-Bunte-Institute, Karlsruhe

Abstract
This work presents further development and validation of the Discrete Ordinates Model for thermal radiation implemented in OpenFOAM® for application to packed beds of particles. The radiation model is an important part of a more comprehensive model for simulating the thermochemical conversion of the discrete phase (here for instance wet biomass particles). The comprehensive Eulerian-Lagrangian model is part of a three-dimensional, time-resolved simulation of the essential chemical and physical processes occurring within and in-between particles in a moving bed.
For the thermal treatment of solid particles, convective and radiative heat transfer couple the energy exchange between the reactor wall, gas- and disperse phase. The original implementation of the finite volume Discrete Ordinate Model (fvDOM) present in OpenFOAM® is valid for a dilute particulate phase and neglects the effect of local opacity due to the existence of individual particles. In the present application, a dense-packed bed of the particulate phase exists in the reactor and, therefore, this direction-based radiation model is adjusted for a computational cell with arbitrary particle volume fractions.
To validate the results with the present thermal radiation model, a simple test case is first presented, where a bed of particles is heated from the top of the computational domain. A second test case relates to an experimentally investigated laboratory-scale reactor. The results of the improved fvDOM are compared to the original implementation in OpenFOAM® and the more simple and computationally cheap P-1 radiation model. In the presence of a packed bed, the P-1 model largely overpredicts the radiative heat transfer while the original fvDOM underpredicts the heat flux by about 15 % for the first test case. The new improved model delivers results within 1% deviation at the expense of maximum of 10 % increase in the computational time.
Large-scale parallel simulations of real setups are crucial tools to predict the efficiency of a process and improve the operational parameters. To achieve the pre-defined product quality at minimum cost, an example of the implemented radiation model in thermochemical conversion of wet biomass in a rotary drum is been given and the importance of the radiation heat transport to the bulk is highlighted.

1. Introduction
The thermochemical conversion of solids is governed by a large number of concurrent physical and chemical processes. They include the motion of the pieces of solids (e.g. biomass, from here on referred to as particles) their heating-up, drying, shrinkage and the primary pyrolysis involving a very large number of chemical reactions. The investigation of these processes is, therefore, complex [1]–[6] and the detailed modeling often requires the use of supercomputers [7]–[10].
A detailed numerical model of particle motion in the framework of the soft-sphere approach, usually called Discrete Element Method (DEM) or Discrete Particle Method (DPM), has been described by Cundall et al. [11] and Tsuji et al. extended the development by considering the effect of fluid on the movement of granular particles in a horizontal pipe [12], [13]. This model considers a collision force between only two neighboring particles, however, neglects the propagation of collision force to further particles. To achieve satisfying precision, the timestep has to be chosen remarkably small. Besides memory limitation for calculation of stiffness for every particle, the restriction on the timestep is a disadvantage resulting in long-time simulations. Independent works of [14] and [15] on 2D laboratory-scale geometries for non-reacting flows show that the computational effort required is 2–4 orders of magnitude higher than that for the Eulerian–Eulerian simulation. Løvås et al. reported that 2D simulation of a small laboratory-size reactor with 40.000 reacting particles in non-reacting flows with a CFD-DPM model using OpenFOAM® lasted 14 days for just 20 s of physical time on a 16-core Intel node [16]. Zhong et al. reported that using models with a detailed particle collision simulation is not suitable for an industrial-scale geometry with 8,000,000 cells and 600,000 particles where it would take 7000 days to calculate 30 s of physical time on a single CPU [8].

A computationally improved stochastic Eulerian-Lagrangian model called Multiphase Particle In Cell (MP-PIC) has drawn the attention for work on large-scale studies. The model is developed by [17] where the original application was originally for dilute phase interactions within a two-way coupled method, but then extended to a four-way coupled model. Similar to the DEM model, the momentum equation is solved for each particle and interactions between particles are considered. In contrast to the DEM model, the particle-particle impact is not calculated individually for each particle but is considered using a pressure tensor for each computational cell. Zhong et al. reported that the computation time for simulating a reacting flow via MP-PIC is only about twice that for the Eulerian–Eulerian simulations and for a case study in their work, MP-PIC was at least 50 times faster than the DEM-based simulation [8].
Another major parameter of the entire process is the heat transport to the packed bed of solid particles. The heat flux through hot walls is required to drive several phenomena in the reactor during the thermal conversion of solids. If a heat carrier medium, e.g. sand, is not involved, the major part of the heat transfer to the solid phase can be assumed to take place via convection and radiation [18]. Convective heat transfer deals with particles and their surrounding gas. The influence of radiation on the operating temperature is not negligible. In this study, the particles are assumed to be perfectly shaped spheres, therefore, impeding the calculation of the contact heat transfer between particles. Based on the results of Zhong et al., the contribution of the contact heat transfer for the bulk in high-temperature moving beds during coal combustion is less than 2 % of the total heat transfer [8]. McCarthy et al. [19] studied the ratio of convective to contact heat transfer in rotary drums with similar parameters as applied in this study and concluded that for conditions of low convective heat transfer coefficients and particles with low thermal conductivity, e.g. biomass, the ratio of convective to conductive heat transfer is above 30.

In [7], we presented details about the utilized Eulerian-Lagrangian approach and performed validations by simulations of both laboratory and industrial-scale rotary kiln reactors. This is realized by combining the particle collision models for non-reactive dense flows with models for heat transport, phase change and chemical reaction for multiphase reacting flow in the framework of OpenFOAM®. Further details of the developed model are presented in [20]. CFD Models of multiphase reactive flow as developed for coal combustion in large boilers [21], [22] or fine spray applications [23], [24] often assume that particles occupy a small volume of the computational cell and are diluted in the gas phase. However, the presence of a packed bed of particles residing at the bottom of the reactor requires special treatment and further developments in each part of the modeling.
The present study deals with the development of radiative heat transfer in packed beds. Particularly, the shadowing effect between particles of the bed is accounted for. The improvements are tested against different radiation models from the literature. Therefore, in the following, a short literature review of the models that handle radiative heat transfer of biomass is presented and their specific strengths and limitations are highlighted.

The lowest-order spherical harmonic method, P-1, is a radiation model suitable for high and homogenous optical thickness and has been used in many research studies and proved to be an acceptable model where homogenous scattering exists [16], [21], [25]–[27]. The P-1 model easily applies to complicated geometries [28]. Its popularity originates from the fact that it solves a partial differential equation for the incident radiation using the same numerical methods as for the other transport equations and is hence easy to solve, but in optically thin media its accuracy can decrease [26], [29]. The equation solved is of diffusion nature and the model cannot handle sharp directional inhomogeneities. Additionally, inaccuracies are observed quite frequently due to the lack of proper boundary conditions [26].

Ku et al. [16] used the P-1 model for simulating the gasification of biomass in fluidized bed reactors stating that this model has generally been chosen in CFD simulations of pulverized fuel gasification with radiation scattering. Their particle model has been of the Lagrangian type and temperatures in the reactor were up to 920 ˚C. Liu et al. [27] applied the P-1 model successfully in a 3D steady-state CFD model to simulate biomass gasification in a circulating fluidized-bed reactor with gas temperatures reaching up to 1000 ˚C. The results showed that the impact of thermal radiation was significant and that thermal radiation needs to be included in the gasification model, however, there was no comparison with measured temperatures in this study.

Klason et al. [26] concluded that the radiative heat transfer rates to the fuel bed are sensitive to the different radiative heat transfer models. For a realistic presentation of the radiative heat transfer to/from the particle bed they suggested applying more computationally demanding models like the grey gas model based on the finite volume discretization (FGG) or, the spectral line weighted-sum-of-grey-gases model (SLW) which, in their study, was also based on finite volumes. The temperature distribution in the furnace obtained with the P-1 model was similar to the other models. However, the trend of the radiative

heat flux to the fuel bed was not realistically captured by the P-1 model which predicted a net heat transfer from the bed to the free-room of the large-scale industry furnace.

Gomez et al. [30] noticed that numerical codes are mature for the simulation of the gas phase but need to be further developed to accommodate also the processes in the solid phase. In their study of biomass combustion within packed beds, they consider the packed bed as a porous medium and modified the original Discrete Ordinate Model (DOM) so that it can account for the temperature difference between the solid and gas phases and the high absorptivity of the medium. Khodaei et al. [31] applied the DOM modification proposed by [30] with the motivation that it can overcome the energy imbalance associated with the standard DOM.

Mehrabian et al. used the DOM together with the weighted sum of grey gases for biomass combustion in the packed bed with a comprehensive validation of multiphysics modeling [32]. They improved the DOM to account for the radiative heat transfer between the particles, the particles and the walls as well as the radiation from the freeboard above the packed bed. The model requires summation over temperatures of neighbor particles within a spherical volume which in general, could turn to be computationally very intensive.

The above-cited papers in the context of DOM use commercial codes for their studies. In the present paper, we apply the open-source code OpenFOAM® to study and validate the radiative part of a new, generally very comprehensive model for thermal conversion of biomass in rotary kiln reactors. The current study applies and compares three models for radiative heat transfer: the P-1 model, the standard DOM as well as the present model accounting for the shadowing effect between neighboring particles. In the two latter models, the Weighted Sum of Gray Gases Model (WSGGM) has been used to model the gas phase with an acceptable compromise between the oversimplified gray gas model and sophisticated models which take particular absorption bands into account.

2. Modeling approach

2.1 Governing equations

The flow of the continuous phase is described by the fully compressible Navier-Stokes equations and numerically solved by using the finite volume method (FVM) within the framework of OpenFOAM [33]. The balance equations for energy and chemical species masses are included as well. Since the focus of this work lies in the modeling of the discrete phase, the reader is referred to [20] for an overview of the numerical description of the continuous phase.

Each biomass particle in the simulation is modeled in a Lagrangian frame of reference. The particles' movement is therefore described by Newton's law, as shown in Eq. 1 considering the external forces $\mathbf{F}$ acting on the biomass particles:

$$m_\mathrm{p} \frac{\mathrm{d}\mathbf{v}_\mathrm{p}}{\mathrm{d}t} = \sum \boldsymbol{F}_\mathrm{external} = \mathbf{F}_\mathrm{c} + \mathbf{F}_\mathrm{g} + \mathbf{F}_\mathrm{d} + \mathbf{F}_\mathrm{p} + \mathbf{F}_\mathrm{v}, \qquad \text{Eq. 1}$$

where $\mathbf{v}_\mathrm{p}$ is the velocity of particle p and m_p its mass. For the forces, collisions between particles or between a particle and the reactor wall ($\mathbf{F}_\mathrm{c}$) are taken into account as well as gravity ($\mathbf{F}_\mathrm{g}$) and the drag force assuming solid spheres ($\mathbf{F}_\mathrm{d}$). Forces due to pressure gradients $\mathbf{F}_\mathrm{p}$and virtual force $\mathbf{F}_\mathrm{v}$ are neglected [24]. With Eq. 1, the particles' position $\boldsymbol{x}_\mathrm{p}$ is then determined from

$$\frac{\mathrm{d}\boldsymbol{x}_\mathrm{p}}{\mathrm{d}t} = \mathbf{v}_\mathrm{p} \qquad \text{Eq. 2}$$

When the wet biomass particles enter the kiln, different physico-chemical processes occur. This entails drying and devolatilization, which leads to a reduction of the particle mass over time. Because of this, the change of particle mass has to be included in the numerical description as well:

$$-\frac{\mathrm{d}m_\mathrm{p}}{\mathrm{d}t} = \frac{\mathrm{d}m_\mathrm{drying}}{\mathrm{d}t} + \frac{\mathrm{d}m_\mathrm{devolatilization}}{\mathrm{d}t} \qquad \text{Eq. 3}$$

The composition of the biomass particles in the numerical model considers moisture, char, ash and volatiles (tar, water, carbon monoxide and carbon dioxide). During the drying phase, moisture is converted from the discrete phase to water vapor and added to the continuous phase. This process is described by a combined model that considers thermal drying and a linearized diffusion-based model [7]. Likewise, during devolatilization, the volatile species are released from the discrete particles to the continuous gas phase. For this, a kinetic model based on experimental measurements is employed [34], [35]. Once the biomass particles are dried and the devolatilization process has finished, the particles finally consist of ash and char with no further reactions occurring. For a more detailed description of the devolatilization and drying models (see [20]).

The change in particle mass due to drying and devolatilization also results in the shrinkage of the particle and a decrease in diameter d_p. In this work, a constant particle density ρ_p is assumed, so that the particle diameter can be computed from:

$$d_\mathrm{p} = \left(\frac{6\, m_\mathrm{p}}{\pi\, \rho_p}\right)^{1/3}, \qquad \text{Eq. 4}$$

Lastly, to describe the temperature of the biomass particles T_p, an energy balance equation for each Lagrangian particle is solved:

$$m_\mathrm{p} c_{p_\mathrm{p}} \frac{\mathrm{d}T_\mathrm{p}}{\mathrm{d}t} = -\dot{Q}_\mathrm{drying} - \dot{Q}_\mathrm{devolatilization} + \dot{Q}_\mathrm{convection} + \dot{Q}_\mathrm{radiation} \qquad \text{Eq. 5}$$

$\dot{Q}_\mathrm{drying}$ is the energy required for the phase change of the water, $\dot{Q}_\mathrm{devolatilization}$ is caused by the endothermic devolatilization process and c_{p_p} is the isobaric heat capacity of the particle, which is a function of the temperature and current particle composition. $\dot{Q}_\mathrm{convection}$ and $\dot{Q}_\mathrm{radiation}$ describe the heat sources due to convection and radiation, which are described in more detail in the following subsection.

2.2 Heat transfer model: convective heat transfer

The accurate modeling of convective heat transfer plays an important role since the particles are assumed to be perfect spheres and therefore do not conduct heat due to direct contact.

A correlation based on the Nusselt number Nu is employed to express the convective heat transfer from Eq. 5 as

$$\dot{Q}_\mathrm{convection} = Nu \cdot \pi \cdot \lambda_\mathrm{g} \cdot d_\mathrm{p} \cdot \left(T_\mathrm{g} - T_\mathrm{p}\right), \qquad \text{Eq. 6}$$

where $\lambda_g$is the thermal conductivity of the continuous gas phase gas mixture and T_g its temperature. The Nusselt number itself is defined as

$$Nu = \frac{h_\mathrm{p} \cdot d_\mathrm{p}}{\lambda_\mathrm{g}}, \qquad \text{Eq. 7}$$

where h_p is the heat transfer coefficient. Due to the generally low gas velocities in the kiln, the Ranz-Marshall model is used to compute the Nusselt number assuming particulate flow with Reynolds numbers less than 5×10^4 [36]:

$$Nu = 2 + 0.6 \cdot {Re_\mathrm{p}}^{\frac{1}{2}} \cdot Pr^{\frac{1}{3}}, \qquad \text{Eq. 8}$$

Re_p is the particle Reynolds number and Pr the Prandtl number.

2.3 Heat transfer model: radiative heat transfer

While the heat transfer due to convection is already available in OpenFOAM, there is no accurate description of heat transfer by radiation for dense particle beds. More specifically, the available models consider the particles to have zero diameter and therefore do not shield each other from radiation. To overcome this, the finite volume discrete ordinates model (fvDOM) has been extended to consider the effect of dense particle beds on radiative heat transfer.

The radiative heat transfer to particles from Eq. 5 is formulated as

$$\dot{Q}_\mathrm{radiation} = \epsilon_\mathrm{p} A_\mathrm{s} \left(\frac{1}{4}\int_{4\pi} I\, d\Omega - \sigma T_\mathrm{p}^4\right), \qquad \text{Eq. 9}$$

where ϵ_p is the particle's emissivity obtained from experiments for particles $\epsilon_\mathrm{p} = 0.70$ and for the wall $\epsilon_\mathrm{w} = 0.85$ [20]. A_s is the projected area of the particle and σ the Stefan-Boltzmann constant. The radiation intensity I is obtained by integration over all directions. In order to calculate the source term of radiation for each particle in a specific computation cell, the radiation source term of the cell must be known. For that, the Radiative Transport Equation (RTE) can be used which describes the propagation of thermal radiation in radiation-active media and integrated over the wavelength written as

$$\frac{\mathrm{d}I}{\mathrm{d}s} = \kappa I_\mathrm{b} - \kappa I - \sigma_s I + \frac{\sigma_s}{4\pi}\int_{4\pi} I\, \Phi\, d\Omega \qquad \text{Eq. 10}$$

where it expresses the change of radiation intensity I over an infinitesimal path length $\mathrm{d}s$. The first term on the right-hand side is the intensity gain through absorption with the absorption coefficient κ related to the medium existing along $\mathrm{d}s$, where I_b stands for black body intensity. The second and the third terms are attenuation through emission and scattering from the path length to other directions with the scattering coefficient σ_s. The fourth term is amplification by scattering from other directions to the path length $\mathrm{d}s$. The difficulty in solving this integrodifferential equation comes from the radiation intensity which is not only dependent on location and time but also the direction. RTE in most of the existing models is simplified as

$$\frac{\mathrm{d}I}{\mathrm{d}s} = \kappa I_{\mathrm{b}} - \kappa I \,. \qquad \text{Eq. 11}$$

neglecting the scattering effect. Discretizing Eq. 11 in space leads to the following equation for each discrete direction in a cell. To solve Eq. 12 numerically, the finite volume discrete ordinates model (fvDOM) is used in OpenFOAM.

$$\frac{1}{V}\sum_{i}^{N}\sum_{k} I_{k_i}(S_i \cdot \hat{\boldsymbol{n}}_k)A_k = -\kappa_{\mathrm{total}} I_{V_i}\Omega_i + \Omega_i\left(\kappa_{\mathrm{g}} I_{\mathrm{bp_g}} + \frac{E_{\mathrm{disperse}}}{4\pi}\right)_V \qquad \text{Eq. 12}$$

The term on the left side represents the sum of values (in this study: rays) on the cell surfaces indexed with k. S_i is the location variable in the direction of the ray i, $\hat{n}_k$ and A are the normal vector and the surface area of the corresponding surface, respectively. The sums express the total amount of incoming radiation from all directions to the specified cell V. The right-hand side of Eq. 12 consists of two terms: one for absorption and another for emission. Ω_i are the discrete directions with solid angles, the former expresses the total absorption of the cell with cell's absorption/emission coefficient κ_{total} and the latter represents the emission which is divided into two parts for the continuous and dispersed phases. To determine the radiation delivered to each particle, Eq. 9 has to be calculated using the numerical solution (Eq. 12) of Eq. 11. For that, the modified absorption/emission coefficient and emission intensity considering densely packed particles are introduced, see the next section.

2.4 Modifications to the fvDOM model

The fvDOM model is valid for calculating the absorption/emission coefficient κ and emission intensity for the dispersed phase, only if the particle volume fraction is low, i.e the sum of the projected area of particles is much smaller than the cell surface. The highlighted restriction in 3D models is that the shading effect in the direction-dependent projected area of particles cannot be considered in control volumes. Therefore, by highly packed cells, the sum of the projected surface of spheres can exceed the real projected area of the cell.

A modification for the determination of the κ, absorption/emission coefficient, for the dense disperse flows is developed and implemented in OpenFOAM®. In this method, the ratio of the cell projected surface to the projected area of all particles within that cell is considered for any arbitrary ray direction Ω_i.

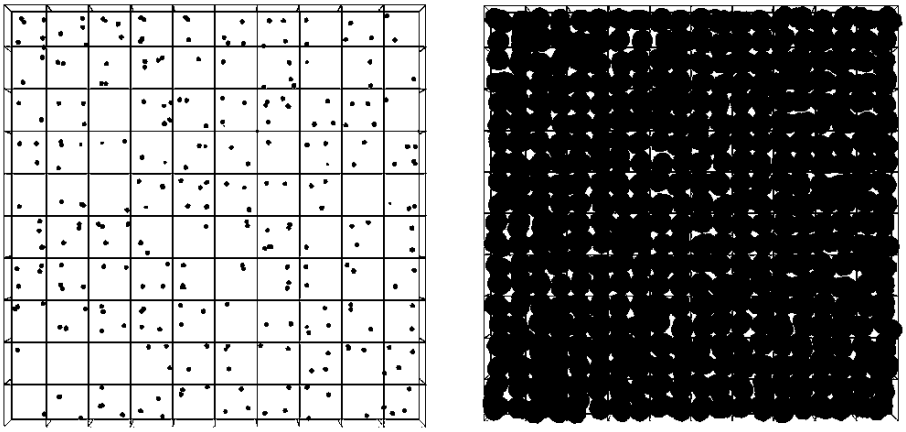

Figure 1 *Comparison of cells' area (in white) and particles' projected area (dark) in the low and high particle volume fraction in cells.*

The left-hand side image in Figure 1 represents a case study with a low ratio of the particles-to-cell projected area where the default equations of OpenFOAM® for κ and emission intensity are valid. The image in the right-hand frame of Figure 1 shows an example case of fully packed particles in multilayers consecutively, in which the sum of the projected area of particles is larger than the cell projected area.

A modification for equations related to the κ_{p} and radiative emission E_{disperse} is suggested to use the minimum and maximum functions in order to return a value with the smaller and larger quantities from the two arguments, respectively.

The calculation of κ_{p} and E_{disperse} should be valid for both possibilities related to the projected area of a cell and its containing particles:

- cells with low particle volume fraction, where $\sum_{i=1}^{n_{\mathrm{pcell}}} A_{\mathrm{p}_i} < A_{\mathrm{pc}}$,

- cells with high particle volume fraction, where $\sum_{i=1}^{n_{\mathrm{pcell}}} A_{\mathrm{p}_i} \geq A_{\mathrm{pc}}$.

n_{pcell} is the number of particles in the corresponding computational cell, A_{pc} is the direction-dependent projected area of the cell and A_{p_i} denotes the projected area of each spherical particle by $A_{\mathrm{p}_i} = \frac{\pi d_{\mathrm{p}_i}^2}{4}$.
The modified equation of the absorption/emission coefficient uses the minimum and maximum functions to return a value with the smaller and larger quantities from the two arguments, respectively.

$$\kappa_{\mathrm{p}} = \frac{A_{\mathrm{pc}}}{V} \frac{\min(A_{\mathrm{pc}}, \sum A_{\mathrm{p}_i})}{\max\{(A_{\mathrm{pc}} - \sum A_{\mathrm{p}_i}),\ A_{\mathrm{small}}\}} \epsilon_{\mathrm{p}} \qquad \text{Eq. 13}$$

The min function in the nominator is responsible for the overlapping effect of particle projected area and ensures that the maximum limit of surface projection (cell projected surface) is not exceeded. This function applies the physical interpretation of shadowing and keeps the intensity balance of cells. The max function in the denominator, on the other hand, ensures the numerical stability and the correct sign of κ_{p} for the circumstance of dense/packed disperse phase. The function prevents division by zero or negative values for κ_{p} through A_{small} as a constant small value. A good compromise between accuracy and numerical stability is found in the value of $A_{\mathrm{small}} = 2.5 \times 10^{-4} A_{\mathrm{pc}}$. The physical interpretation of very large κ_{p} means entire absorption of the incoming radiation intensity.
A similar principle has to be applied for the modification of radiative emission from particles in cells.

$$E_{\mathrm{disperse}} = \min\left(1, \frac{A_{\mathrm{pc}}}{\sum A_{\mathrm{p}_i}}\right) \cdot \sigma \frac{\epsilon_{\mathrm{p}}}{V} \sum_{i=1}^{n_{\mathrm{pcell}}} A_{\mathrm{s}_i} T_{\mathrm{p}_i}^4 \qquad \text{Eq. 14}$$

The min function in Eq. 14 takes the shading effect of particles into account. As long as the sum of the projected area of particles is less than the cell surface, the function applies unity values and acts neutrally. If the cell is densely packed, the ratio $\frac{A_{\mathrm{pc}}}{\sum A_{\mathrm{p}_i}}$ can be smaller than one and therefore the function applies a factor less than one to fulfill the shading effect of the total emission. The factor basically considers a part of the emission that finds no way to leave the cell and is absorbed by neighboring particles.

2.5 Overview of numerical methods

The presented solver in this work is based on the described coupling and developed submodels from previous works [7], [20], [37], [38]. A simplified numerical scheme of the developed solver during one timestep is shown in Figure 2. Calculations for each phase are sketched in separate blocks. Mass, momentum and energy exchange between phases are handled through source terms. Regarding the discrete phase, for the particle collision, the MP-PIC model is used assuming that parcels (i.e. computational clusters) are made up of uniform groupings of particles, where they share the same physical properties in the parcel. Further details regarding the particle collision model can be found in [20].

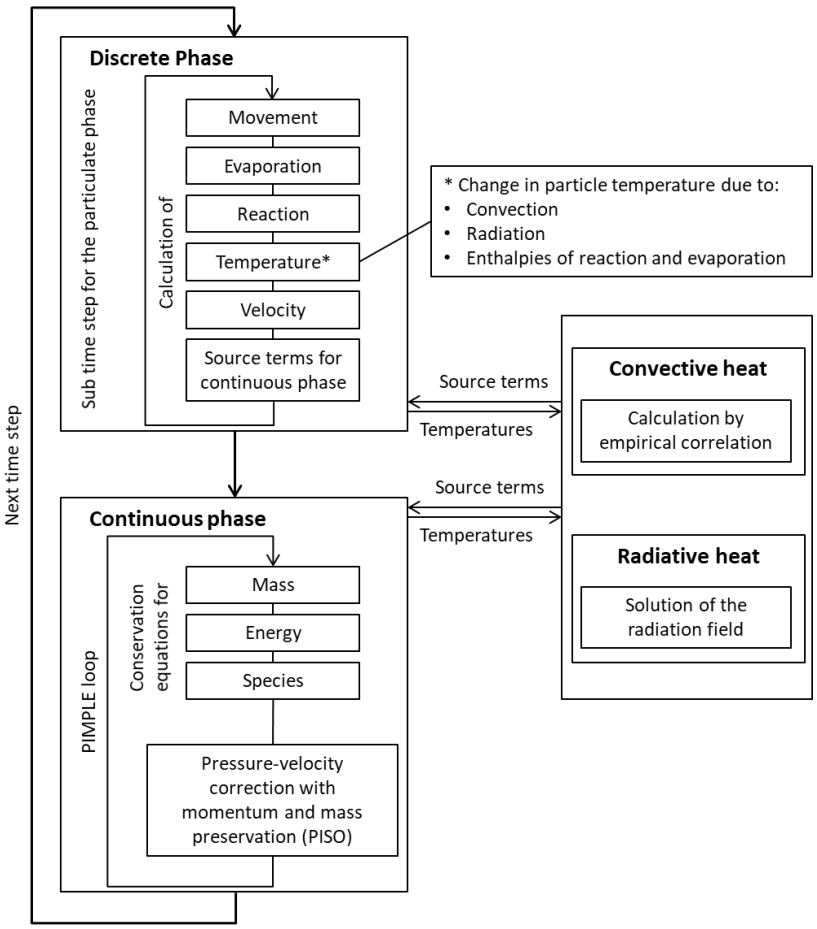

Figure 2 *Simplified numerical flowchart of the solver for one timestep.*

3. Results and discussion

3.1 Validation of the extended radiation model for dense particle flows

The improvements of OpenFOAM's fvDOM model are validated with two configurations for the consideration of dense particle flows. First, a simple test case is employed, where a box of side length 20 cm is filled with a bed of equally sized particles with 6 mm diameter, assuming no convection (i.e. vacuum box). The particle diameter coincides with the computational cell size, representing the limiting case of high particulate volume fractions. In total, 1800 particles with an initial temperature of 373 K are placed into the box and form a bed of several layers or a height of 2 cm. All sides of the box are walls with a temperature of 373 K. To evaluate the behavior of the new radiation model, the temperature of the top wall is set to 673 K. The setup is shown in Figure 3 on the left.

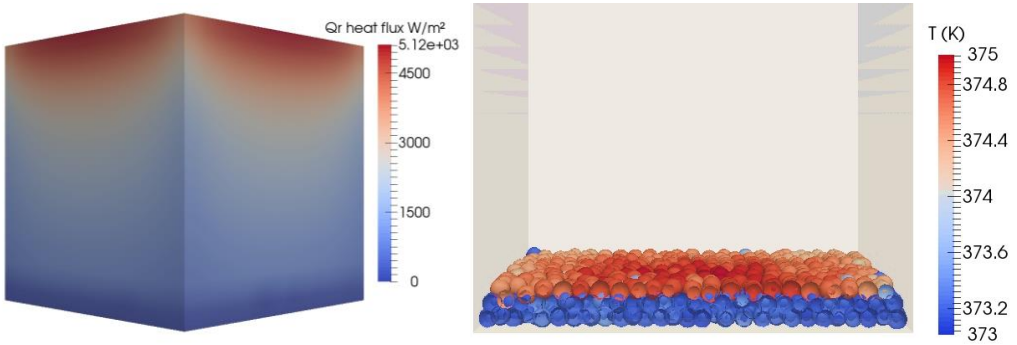

Figure 3 *Setup of the numerical test case. A box with hot top wall (left) is used to investigate the radiative heat transfer to bed particles (right).*

When the simulation is started, the radiation from the top wall heats the top layer of the particle bed, as shown in Figure 3 on the right. The new implementation considers the volume fraction of particles and projected area in the computational cells and thus the top particle layer shields the lower layers from the radiation from the ceiling.

The simulation is stopped after a physical time of 11 s. The total heat flux from the top wall to the particles can be determined by the increase of temperature from all particles and the heat flow can be calculated as

$$\dot{Q}_{p_{total}} = \dot{Q}_{\text{radiation}} = \frac{1}{\Delta t}\sum_i m_i c_{p_i} \Delta T_i \qquad \text{Eq. 15}$$

where $\dot{Q}_{p_{total}}$ is the total heat flux from the wall to the particles, Δt the simulation time and ΔT_i the change of temperature of particle i.

Due to the simple setup, a view factor model can be used to estimate the expected heat flux. Assuming the top particle layer as a plane with the side length of 20 cm and a distance to the top wall of 18 cm yields a view factor between the top particle layer and the top wall of $F_{1\to 2} = 0.2286$, calculated from [29]. With this, the heat flux based on the view factor methodology can be expressed as

$$\dot{Q}_{\text{radiation}} = \sigma\, F_{1\to 2}\, 0.20^2\ \text{m}^2\left(T^4_{top\ wall} - T^4_{top\ layer}\right) \qquad \text{Eq. 16}$$

where the $T_{top\ wall}$ and $T_{top\ layer}$ are the temperature of the upper wall and the initial temperature of the uppermost particle layer respectively. Note that, for this simulation, the side walls are isotherm and fixed at the initial temperature of particles T_{p}.

Table 1 *Radiation heat delivered to particles over time in a box with 1800 particles: comparison of different models with view factor calculation.*

Heat (W)	View factor model	fvDOM (improved)	fvDOM	P-1
To particles	96.3	97.4	82.6	288.9
From all walls	96.3	96.7	82.4	289.5

Table 1 compares the estimated value of $\dot{Q}_{\text{radiation}}$ from the view factor estimation in Eq. 15 with the simulation result from the improved fvDOM implementation. The improved fvDOM model yields excellent agreement within 1 % of the estimated heat flux with the view factor estimate. If the simulation is instead performed with OpenFOAM's original fvDOM model without considering the shielding effect of the particles, the heat flux is underestimated by about 15 %. About 12.6 W of radiative heat flow reaches the bottom wall of the box when using the standard fvDOM Model, even though the bottom wall is fully covered by a dense particle bed. Even worse results are achieved by using the P-1 radiation model, which overestimates the heat flow by a factor of three. The reason is that the P-1 model is not well suited for cases with heterogeneous optical obstructions and with strongly anisotropic distribution of radiation intensity. As shown in Figure 4, the particle bed in a rotary kiln represents such an anisotropic case.

3.2 Validation of radiative heat transport in the rotating tube

A more complex test case is given by an experimentally investigated rotary kiln with a length of 1.4 m and an outer diameter of 8.5 cm by Carbolite Gero Ltd. (UK). The rotating tube is surrounded by an electric furnace, covering a length of 1 m. In the simulation, the same geometry as in the experimental setup is used. 1700 monodisperse particles with a diameter of 6 mm are inserted into the tube in the simulation and the tube walls are assumed to have a constant temperature of 673 K, while the particles have an initial temperature of 320 K. The simulations have been run for 11 seconds and the results from the last 10 seconds have been evaluated. In the large-scale setup (section 3.4), a realistic particle size distribution between 1 and 9 mm in diameter with mean of 6 mm and a variance of 2 is defined [7].

As in the previous test case of a particle bed in a box, the simulation of the particle bed in the kiln is performed with the improved fvDOM model, the standard fvDOM model and the P-1 radiation model. Figure 4 shows snapshots from the particle bed inside the kiln. On the top left, the position of the particles inside the reactor tube is shown. On the top right, the radiative heat flux at the kiln wall is shown for the simulation using the P-1 model. The radiative heat flux at the reactor walls from the improved fvDOM model is shown on the bottom left and the heat flux from the standard fvDOM model on the bottom right.

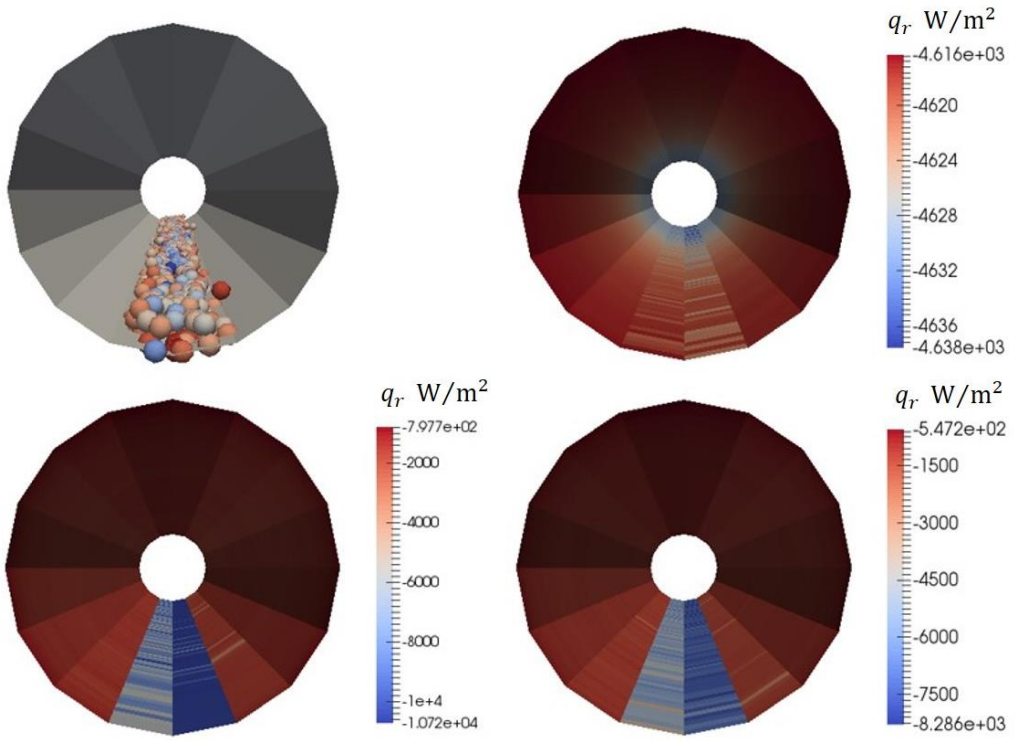

Figure 4 *Particle bed in the rotary kiln (top left), radiative heat flux q_r from the simulations using the P-1 model (top right), the improved fvDOM model (bottom left) and standard fvDOM model (bottom right).*

The result from the P-1 model shows that the heat flux distribution is uniform in the circumferential direction. This means, that the P-1 model does not take the presence of the particles into account. For both the improved and original fvDOM model (bottom pictures in Figure 4), the presence of the particle bed influences the predicted heat fluxes. For the simulation with the improved model, the heat flux from the bottom part of the kiln to the particle bed is about $\dot{q}_r = -1.07 \times 10^4$ W/m², while for the original fvDOM model it is $\dot{q}_r = -8.29 \times 10^3$ W/m². The expected heat flux can again be estimated, by considering the maximum possible heat flux (calculated with the temperature of the coldest particle) from the Stefan-Boltzmann law:

$$\dot{q}_{r,max} = \sigma\left(T_{wall}^4 - T_{p_{min}}^4\right) = 10949\,\frac{\mathrm{W}}{\mathrm{m}^2} \qquad \text{Eq. 17}$$

Table 2 *Heat delivered from the hot kiln walls to the particle bed over time from the simulation using the improved fvDOM model from this work, the standard fvDOM model and the P-1 model as well as computing time.*

Model	$\dot{Q}$ (W)	computing time (s)	$T_{p\,min}$ (K)	$T_{p\,max}$ (K)
Improved fvDOM	930	2199	331.3	349.7
fvDOM	671	1990	328.8	345.7
P-1	1625	502	352.1	354.1

Table 2 summarizes the total heat flow from the kiln walls to the particle bed. Similar to the previous test case, the standard fvDOM model underestimates the heat flow to the particle bed, while the P-1 model overestimates it. In the kiln geometry, the difference between the original and improved fvDOM model is about 30 % and therewith much larger than in the simplified case of particles in a box, which highlights the need for accurate radiation modeling for more complex and realistic cases.

One critical aspect of radiation modeling is computational performance. The new fvDOM model for dense particulate flows requires additional computations based on particle properties and distribution. **Table 3**The comparison between the original and improved model in the table shows that the increase in simulation time is acceptable, with an overall increase of about 10 % while the total heat flow has a considerebale change of around 38%. The simple P-1 model yields much faster simulation times, but with inadequate results. The computational efficiency of the model is an important factor since the final simulation in the large-scale model should run for a physical time of 3000 seconds.

3.3 Computational performance of the radiation model

The resolved DOM radiation models are computationally very intensive and, therefore, they have a direct impact on the computational efficiency of the simulation. This effect can be high enough to

turn the large-scale simulation into an infeasible case in terms of computational cost, even on parallel runs with several hundreds of processors. Therefore, precise investigation to reduce the computational effort with an acceptable precision is necessary.

Table 3 *Computing time and heat delivered to particles over time during a one-hour physical time simulation in a laboratory-scale reactor, a parallel run with 16 processors.*

Discrete directions	Solver freq.	Computation time for each processor (s)	$\dot{Q}_{wall}$ (W)	Relative deviation (%)
128	1	62100	211.97	0
72	1	37543	215.53	2.69
72	10	10111	216.69	2.39
72	20	8775	216.84	2.50
-	deactivated	6671	0	Not defined

Table 3 gives an overview of the results from a series of simulations for the parallel run with 16 processors carried out on the realistic physical time scale for the Carbolite Gero geometry with adjusted and finalized submodels and parameters. As it can be interpreted, the total number of discrete directions, as well as the setting *solver frequency* (which determines the recalculation frequency of the radiation field) have a decisive influence on the computing time. The results suggest that, for the application of well-mixed beds, the solver frequency is more effective on the computational effectivity rather than the number of directions. Therefore, the number of discrete directions is kept as high as possible, and the displayed results of only 128 and 72 directions are tabulated here. The results for lower numbers of directions have been ignored since the computation time is not distinctly lower for a comparable solver frequency whereas the accuracy is remarkably diminished. The mean deviation is calculated from the reference case with 128 directions and the radiation solver frequency of one. The relative deviation is calculated for each data point and averaged over time.

In the adjusted settings for the large-scale simulations, the 72 global spatial directions for ray-tracing are used to calculate the radiation field in each 20th timestep, This results in an acceptable average deviation of 2.5 % from the reference case with a 7 times faster simulation.

3.4 Application of the radiation model on large-scale simulations

The developed and validated radiation model in this study has been implemented in an adjusted solver in OpenFOAM to study the effectiveness of the reactor design and product quality and presented in the previous work [7]. As can be seen in Figure 5 a, the model has been implemented in the large-scale reactor with a diameter of 1.2 m and length of 12 m. the wet-particle bulk (initial moisture content of 50 wt.%) takes very long to be dried and this can be interpreted from the particle temperature along the reactor. More than two-thirds of the length of the reactor is used for drying as the particle temperature is below the boiling point of water, despite the contact with the hot wall. The large temperature difference between the bulk and reactor wall emphasizes the influence of the radiation heat transfer. Another evidence of the importance of radiation heat transfer is the gas temperature along the reactor (Figure 5 b), which shows a stratification effect against the diameter of the reactor. This is due to the low gas flow velocity in the reactor and therefore prevents radial mixing of the gas phase. The stratification of the gas phase increases the thermal resistance against the convective heat transport to the bed and since the relative temperature of the bed and surrounding gas is not at its highest, convective heat transfer does not have the highest efficiency compared with technologies like fluidized bed reactors.

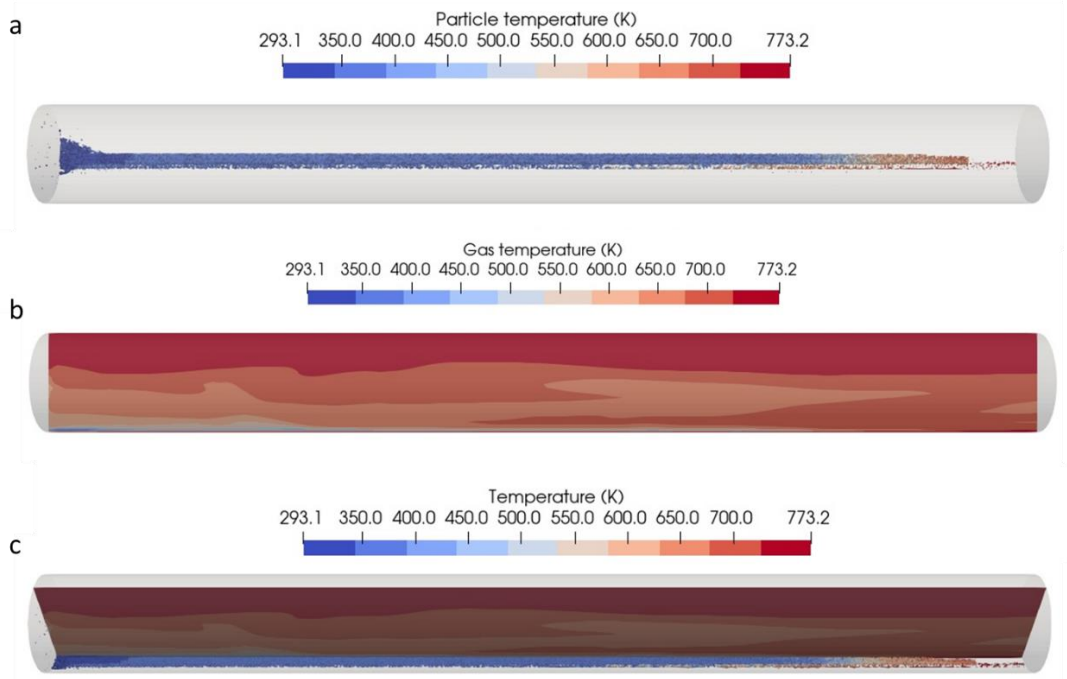

Figure 5 simulation of thermal conversion of wet particles in an indirectly heated rotary drum reactor with a diameter of 1.2 m and length of 12 m; feed throughput from left-side. a) top-view representing the particle temperature distribution along the reactor. b) Gas temperature distribution, side-view on a cutting plane through the center of the reactor c) Gas-particle temperature in one frame, side-view with 45° angle view. Particles are shown as spheres colored by Temperature.

4. Summary and Conclusions

Simulations of pyrolysis in rotary kilns is a challenging task due to many different physical processes governing the conversion of biomass to char. It requires the modeling of moisture evaporation, devolatilization as well as the interaction of biomass particles with each other to simulate the formation of particle beds. An improved solver based on the open-source framework OpenFOAM has been developed that includes models for all relevant processes and allows the simulation of the gas phase inside the kiln together with the particulate phase in a fully coupled manner. In industrial realizations of rotating indirectly heated kilns, radiative heat transfer plays an important role. Because of this, accurate radiation models are mandatory. However, commonly used radiation models are not formulated for multiphase flows and do not consider particle shielding. In this work, an extension of the finite volume discrete ordinate model (fvDOM) has been developed that takes into account the volume fraction of the particulate phase in each computational cell and thus models the correct heat flux due to radiation to particle beds. A simple test case of a particle bed in a box heated from the top wall shows a realistic result and yields a deviation of about 1 % from the expected heat flux. Without the new development, the heat flux is underestimated by 15 % and radiation from the top wall reaches the bottom wall, even though it is covered by large particles in several layers. The P-1 radiation model has shown to be inadequate due to the anisotropy introduced by the particle bed. The validation of the new model is carried out. Additionally, an application to a real kiln geometry has been simulated by showing the improved modeling of radiative heat fluxes compared with the original fvDOM and P-1 models. The developed radiation model shows an important improvement in the predictive quality of biomass pyrolysis simulations in rotating kilns with acceptable computational overhead.

Acknowledgment

The Authors would like to thank sincerely Mr. Niklas Weber for his insightful and scientific input, which have given during his Master's thesis at Engler-Bunte-Institute. The basic idea and code adjustment could not have existed without the valuable efforts of Mr. Weber.

References

[1] C. Di Blasi, "Modeling chemical and physical processes of wood and biomass pyrolysis," *Prog. Energy Combust. Sci.*, vol. 34, no. 1, pp. 47–90, Feb. 2008, doi: 10.1016/j.pecs.2006.12.001.

[2] W. C. Park, A. Atreya, and H. R. Baum, "Experimental and theoretical investigation of heat and mass transfer processes during wood pyrolysis," *Combust. Flame*, vol. 157, no. 3, pp. 481–494,

Mar. 2010, doi: 10.1016/j.combustflame.2009.10.006.

[3] A. Williams, M. Pourkashanian, and J. M. Jones, “Combustion of pulverised coal and biomass,” *Prog. Energy Combust. Sci.*, vol. 27, no. 6, pp. 587–610, 2001, doi: 10.1016/S0360-1285(01)00004-1.

[4] F. Wissing, S. Wirtz, and V. Scherer, “Simulating municipal solid waste incineration with a DEM/CFD method – Influences of waste properties, grate and furnace design,” *Fuel*, vol. 206, pp. 638–656, Oct. 2017, doi: 10.1016/j.fuel.2017.06.037.

[5] A. Sharma, V. Pareek, S. Wang, Z. Zhang, H. Yang, and D. Zhang, “A phenomenological model of the mechanisms of lignocellulosic biomass pyrolysis processes,” *Comput. Chem. Eng.*, vol. 60, pp. 231–241, Jan. 2014, doi: 10.1016/j.compchemeng.2013.09.008.

[6] A. Anca-Couce, “Reaction mechanisms and multi-scale modelling of lignocellulosic biomass pyrolysis,” *Prog. Energy Combust. Sci.*, vol. 53, no. 2016, pp. 41–79, Mar. 2016, doi: 10.1016/j.pecs.2015.10.002.

[7] S. Tavakkol *et al.*, “An Eulerian-Lagrangian method for wet biomass carbonization in rotary kiln reactors,” *Renew. Sustain. Energy Rev.*, vol. 139, p. 110582, Apr. 2021, doi: 10.1016/j.rser.2020.110582.

[8] W. Zhong, A. Yu, G. Zhou, J. Xie, and H. Zhang, “CFD simulation of dense particulate reaction system: Approaches, recent advances and applications,” *Chem. Eng. Sci.*, vol. 140, pp. 16–43, 2016, doi: 10.1016/j.ces.2015.09.035.

[9] H. P. Zhu, Z. Y. Zhou, R. Y. Yang, and A. B. Yu, “Discrete particle simulation of particulate systems: Theoretical developments,” *Chem. Eng. Sci.*, vol. 62, no. 13, pp. 3378–3396, 2007, doi: 10.1016/j.ces.2006.12.089.

[10] H. P. Zhu, Z. Y. Zhou, R. Y. Yang, and A. B. Yu, “Discrete particle simulation of particulate systems: A review of major applications and findings,” *Chem. Eng. Sci.*, vol. 63, no. 23, pp. 5728–5770, 2008, doi: 10.1016/j.ces.2008.08.006.

[11] P. A. Cundall and O. D. L. Strack, “A discrete numerical model for granular assemblies,” *Géotechnique*, vol. 29, no. 1, pp. 47–65, Mar. 1979, doi: 10.1680/geot.1979.29.1.47.

[12] Y. Tsuji, T. Tanaka, and T. Ishida, “Lagrangian numerical simulation of plug flow of cohesionless particles in a horizontal pipe,” *Powder Technol.*, vol. 71, no. 3, pp. 239–250, 1992, doi: 10.1016/0032-5910(92)88030-L.

[13] K. Yamane, M. Nakagawa, S. A. Altobelli, T. Tanaka, and Y. Tsuji, “Steady particulate flows in a horizontal rotating cylinder,” *Phys. Fluids*, vol. 10, no. 6, pp. 1419–1427, Jun. 1998, doi: 10.1063/1.869858.

[14] L. Li, B. Li, and Z. Liu, “Modeling of spout-fluidized beds and investigation of drag closures using OpenFOAM,” *Powder Technol.*, vol. 305, no. October, pp. 364–376, 2017, doi: 10.1016/j.powtec.2016.10.005.

[15] F. Ronsse, R. W. Nachenius, and W. Prins, “Carbonization of Biomass,” in *Recent Advances in Thermo-Chemical Conversion of Biomass*, Elsevier, 2015, pp. 293–324.

[16] X. Ku, T. Li, and T. Løvås, “CFD-DEM simulation of biomass gasification with steam in a fluidized bed reactor,” *Chem. Eng. Sci.*, vol. 122, pp. 270–283, 2015, doi: 10.1016/j.ces.2014.08.045.

[17] D. M. Snider, P. J. O’Rourke, and M. J. Andrews, “An Incompressible Two-Dimensional Multiphase Particle-In-Cell Model for Dense Particle Flows,” Los Alamos National Laboratory, 1997.

[18] P. N. Ciesielski *et al.*, “Advances in Multiscale Modeling of Lignocellulosic Biomass,” *ACS Sustain. Chem. Eng.*, vol. 8, no. 9, pp. 3512–3531, Mar. 2020, doi: 10.1021/acssuschemeng.9b07415.

[19] D. Shi, W. L. Vargas, and J. J. McCarthy, “Heat transfer in rotary kilns with interstitial gases,” *Chem. Eng. Sci.*, vol. 63, no. 18, pp. 4506–4516, 2008, doi: 10.1016/j.ces.2008.06.006.

[20] S. Tavakkol, “Numerical Simulation of Wet Biomass Carbonization in Tubular Reactors,” Karlsruhe Institute of Technology (KIT), PhD Thesis, DOI:10.5445/IR/1000134976 , 2021.

[21] J. Xie, W. Zhong, Y. Shao, Q. Liu, L. Liu, and G. Liu, “Simulation of Combustion of Municipal Solid Waste and Coal in an Industrial-Scale Circulating Fluidized Bed Boiler,” 2017, doi: 10.1021/acs.energyfuels.7b02693.

[22] H. Zhou, G. Flamant, and D. Gauthier, “DEM-LES simulation of coal combustion in a bubbling fluidized bed Part II: coal combustion at the particle level,” *Chem. Eng. Sci.*, vol. 59, no. 20, pp. 4205–4215, Oct. 2004, doi: 10.1016/j.ces.2004.01.070.

[23] C. T. Crowe, M. P. Sharma, and D. E. Stock, “The Particle-Source-In Cell (PSI-CELL) Model for Gas-Droplet Flows,” *J. Fluids Eng.*, vol. 99, no. 2, p. 325, 1977, doi: 10.1115/1.3448756.

[24] C. T. Crower, J. D. Schwarzkopf, M. Sommerfeld, and Y. Tsuji, *Multiphase with Droplets Flows wnd Particles*. CRC Press Taylor & Francis Group, 2012.

[25] S. S. Sazhin, E. M. Sazhina, O. Faltsi-Saravelou, and P. Wild, “The p-1 model for thermal radiation transfer: Advantages and limitations,” *Fuel*, vol. 75, no. 3, pp. 289–294, 1996, doi: 10.1016/0016-2361(95)00269-3.

[26] T. Klason, X. S. Bai, M. Bahador, T. K. Nilsson, and B. Sundén, “Investigation of radiative heat transfer in fixed bed biomass furnaces,” *Fuel*, vol. 87, no. 10–11, pp. 2141–2153, 2008, doi: 10.1016/j.fuel.2007.11.016.

[27] H. Liu, A. Elkamel, A. Lohi, and M. Biglari, “Computational fluid dynamics modeling of biomass gasification in circulating fluidized-bed reactor using the eulerian-eulerian approach,” *Ind. Eng. Chem. Res.*, vol. 52, no. 51, pp. 18162–18174, 2013, doi: 10.1021/ie4024148.

[28] R. I. Backreedy, L. M. Fletcher, L. Ma, M. Pourkashanian, and A. Williams, “Modelling pulverised coal combustion using a detailed coal combustion model,” *Combust. Sci. Technol.*, vol. 178, no. 4, pp. 763–787, 2006, doi: 10.1080/00102200500248532.

[29] M. F. Modest, *Radiative heat transfer*, Second ed. San Diego: Academic Press (Elsevier), 1993.

[30] M. A. Gómez, J. Porteiro, D. Patiño, and J. L. Míguez, “CFD modelling of thermal conversion and packed bed compaction in biomass combustion,” *Fuel*, vol. 117, no. PART A, pp. 716–732, 2014, doi: 10.1016/j.fuel.2013.08.078.

[31] H. Khodaei, L. Gonzalez, S. Chapela, J. Porteiro, P. Nikrityuk, and C. Olson, “CFD-based coupled multiphase modeling of biochar production using a large-scale pyrolysis plant,” *Energy*, vol. 217, p. 119325, 2021, doi: 10.1016/j.energy.2020.119325.

[32] R. Mehrabian, A. Shiehnejadhesar, R. Scharler, and I. Obernberger, “Multi-physics modelling of packed bed biomass combustion,” *Fuel*, vol. 122, no. 2014, pp. 164–178, 2014, doi: 10.1016/j.fuel.2014.01.027.

[33] C. Greenshields and The OpenFOAM Foundation, “OpenFOAM User Guide,” *OpenFOAM Foundation*, 2019. https://cfd.direct/openfoam/user-guide/.

[34] M. Müller-Hagedorn, H. Bockhorn, L. Krebs, and U. Müller, “A comparative kinetic study on the pyrolysis of three different wood species,” *J. Anal. Appl. Pyrolysis*, vol. 68–69, pp. 231–249, 2003, doi: 10.1016/S0165-2370(03)00065-2.

[35] M. Müller-Hagedorn and H. Bockhorn, “Pyrolytic behaviour of different biomasses (angiosperms) (maize plants, straws, and wood) in low temperature pyrolysis,” *J. Anal. Appl. Pyrolysis*, vol. 79, no. 1-2 SPEC. ISS., pp. 136–146, 2007, doi: 10.1016/j.jaap.2006.12.008.

[36] N. Wakao, S. Kaguei, and T. Funazkri, “Effect of fluid dispersion coefficients on particle-to-fluid heat transfer coefficients in packed beds. Correlation of Nusselt numbers,” *Chem. Eng. Sci.*, vol. 34, no. 3, pp. 325–336, 1979, doi: 10.1016/0009-2509(79)85064-2.

[37] S. Tavakkol, T. Zirwes, J. A. Denev, N. Weber, and H. Bockhorn, “Development and validation of an Euler-Lagrange method for the numerical simulation of wet-biomass carbonization in a rotary kiln reactor,” *29. Dtsch. Flammentag*, 2019.

[38] S. Tavakkol, T. Zirwes, J. A. Denev, F. Jamshidi, and H. Bockhorn, “Development of an Openfoam Solver for Numerical Simulation of Carbonization of Biomasses In Rotary Kilns,” in *15th OpenFOAM Workshop*, 2020, pp. 1–8.